# RSC Advances

ROYAL SOCIETY OF CHEMISTRY

www.rsc.org/advances

# Journal Name

## ARTICLE

# Effect of glass frit in Ag paste on the electrical properties of front-side Ag contacts for crystalline-silicon solar cells

Yuping Tai [a] , Guojun Zheng [a] , Hanying Wang[b], Hui Wang [a, b,] *, Jintao Bai [b]

## Abstract

The effect of glass frit, used in front-side silver pastes, on the electrical properties of front-side silver contacts in silicon solar cells was studied. Glass frits with the same composition, but three different degrees of crystallization were prepared by introducing some nucleating agents to provide nucleation sites for the formation of the crystal structure glass-frit. The phase structure of the glass frits was characterized by X-ray diffraction. The Ag-Si contacts were demonstrated by scanning electron microscopy, and the results indicated that the glass frit with moderate crystallization degree was facilitated to acquire optimal size crystalline Ag that distributed uniformly in the glass layer and silicon substrate. Therefore, the excellent metallization contact were achieved. In addition, the particle size and proportion of glass frit in the paste also had an impact on the electrical properties of solar cells. The results indicated that a silver paste consisting of 3 wt% crystalline glass frit with a particle size of 3.12 µm not only ensured sufficient adhesion of the silver electrode, but also improved the Ag-Si contact to enhance the conversion efficiency of solar cells.

a. *Key Laboratory of Synthetic and Natural Functional Molecule Chemistry (Ministry of Education), College of Chemistry and Materials Science, Northwest University, Xi'an 710069, P. R. China*

b. *National Key Laboratory of Photoelectric Technology and Functional Materials (Culture Base), National Photoelectric Technology and Functional Materials and Application of International Science and Technology Cooperation Base, Institute of Photonics & Photon-Technology, Northwest University, Xi'an 710069, P. R. China*

*\*E-mail address: huiwang@nwu.edu.cn (Hui Wang) Tel.: +86 029 88363115*

*fax: +86 029 88302571*

## Introduction

With the increasing concerns regarding environmental pollution and global climate change, more attention is paid to the development and utilization of new energy resources. Crystalline-silicon solar cells are a main source of alternative energy because of their high efficiency and low cost.[1-4] Screen-printed thick-film silver metallization is widely used for the front-side contacts of silicon solar cells because it is more cost- and time-effective than other metallization techniques such as photolithography or light-induced electroplating.[5,6] In general, a silver paste primarily consists of three constituents:[7-9] (a) a powder of silver particles, which provides the conductive phase for collecting electrons owing to silver's superior conductivity among the noble metals; (b) glass frit, as a binder phase to adhere the silver phase to the silicon substrate and ensure the formation of Ag-Si contact; (c) an organic medium, which disperses the silver powder and glass frit to obtain a good aspect ratio of grids required to attain the desired rheological properties for the paste.

Several studies[10-12] have reported the role of glass frit in Ag-Si contact formation. During firing, the fluidized glass frit is known to etch through the $SiN_x$ antireflection coating (ARC) and react with the silicon emitter, which enables silver crystallites to nucleate at the glass/Si interface to form an electrical contact with the emitter. The distribution and size of the silver crystallites formed at the silicon emitter interface are believed to be important factors for achieving good-quality ohmic contact with the emitter.[13,14] Ballif et al.[15] reported that the most appropriate size of silver crystallites is around 200-500 nm. The small silver crystallites cannot adequately penetrate the silicon substrate to form a good ohmic contact with the silicon substrate, and the silver crystallites that overgrow into the emitter can cause junction shunting. In addition, Li etal.[16]

confirmed that a glass layer was formed between the silicon substrate and bulk silver in their study. Because the glass layer thickness is critical to the tunneling mechanism of current flow,[17] Li et al.[18] proposed a plausible tunneling conduction model is proposed in which photoelectrons are extracted from the silicon emitter through a thin interfacial glass layer that is richly decorated with nanoscale silver colloids.[19] Therefore, an ideal Ag-Si eutectic structure at the interface between the silver and silicon layers for crystalline-silicon solar cells requires silver crystallites of an appropriate size and a glass layer of an appropriate thickness.

In this work, we focused on the preparation of a functional glass frit that could crystallize in the sintering process. This kind of glass frit can freeze the glass at an early stage to prevent silver crystallites from fully precipitating from the glass to form thinner glass regions. We also used scanning electron microscopy (SEM) and X-ray diffraction (XRD) to study the nucleation mechanism of the crystalline glass frit to determine the route to form an ideal Ag-Si eutectic structure. In addition, we studied other factors through which the glass frit can affect the electrical performance of a silver paste, such as the particle size of the glass frit and the content of glass frit in the paste. Finally, this paper will present a few ways to optimize the silver-paste material for forming high-quality front contacts in crystalline-silicon solar cells.

## Experimental

### Synthesis of glass-frit powders

The glass frit powders were prepared by traditional melting. A uniform stoichiometric oxide mixture consisting of PbO, $TeO_2$, $SiO_2$, CaO, and $Al_2O_3$ was heated in an aluminum crucible placed in a 1200°C muffle furnace for 1.5 h. The melt was then removed rapidly from the furnace and poured into deionized water to cool to room

temperature. After grinding by ball milling for different cycles (measured in hours), a series of glass frit powders with different sizes was prepared.

### Synthesis of organic medium

The organic medium was prepared by mixed solvents, thixotropic agents, surfactant and coupling agent. The solvents (methyl carbitol, N-butyl butyrate, terpineol, triethanolamine), thickener (EC), thixotropic agents, surfactant (sorbitan trioleate), and coupling agent (silane coupling agent KH-570) were added into three-necked flask successively. The materials completely dissolved around 90-110° C in a water bath by stirring for 3h and then cooled to room temperature.

### Synthesis of crystalline silver

In a typical procedure, silver nitrate and ascorbic acid were dissolved in deionized water, respectively. Gelatin was dissolved in both of these solutions according to stoichiometric ratio subsequently. The silver nitrate and gelatin solution was added to the ascorbic acid and gelatin solution slowly, and stirred for 30 min at the same time. The pH of reaction system was controlled by using aqueous ammonia during the reaction process. Finally, the silver particles were filtrated and washed with alcohol to remove impurities and then dried at 70° C for 8 h.

### Synthesis of silver paste

The silver paste was prepared by mixing the as-prepared microscale Ag crystalline particles, glass frit powder with specific size, and organic medium, using a three-roll mixer. This process was intended to produce silver pastes by using different glass frit with different crystalline degree, particle size and proportion, while the Ag particles and the organic medium remained unchanged. During the mixing procedure, the organic medium was responsible for wetting and dispersing silver particles and glass frits

homogeneously, and then the silver pastes with optimal viscosity and thixotropy were acquired. Crystalline Si solar cells were then fabricated using the different silver pastes mentioned above on single-crystalline Cz-Si wafers (125 mm × 125 mm) with an emitter whose resistivity was approximately 60 Ω/sq, experience the screening print and high-temperature firing step. The organic medium evaporated during the drying and firing step.

### Measurements

The crystal structure of silver particles and the glass-frit powders were characterized with an X-ray diffractometer (D/Max-3C, Rigaku, Japan) using Cu $K_\alpha$ radiation. The morphology of silver particles, the glass-frit powders and silver-electrode samples were examined using a scanning electron microscope (JSM-6390, JEOL, Japan). The distribution of glass frit's particle size was measured by laser particle analyzer (Mastersizer 3000, Malvern). The welding tension between silver electrode and Si substrate was measured by FDV-50 force apparatus (Wagner Instruments, USA).

The surface morphology of the cells was obtained by chemical etching, which consisted of two steps: (a) etching by aqua regia (32% HCl, 65% $HNO_3$, v/v of 3:1; $t$ = 1 h) to remove silver from the finger bulk, leaving the glass layer at the emitter surface; (b) subsequent etching of the glass layer by a 3% HF solution for 10 min at room temperature, leaving the Ag crystallites grown in the emitter. The conversion efficiency of the single-crystalline Cz-Si solar cells was measured by battery testing equipment (ITA, Baccini Applied Materials, Italy/USA).

## Results and discussion

### Crystal structure and morphology of silver particles

Fig. 1 displayed the XRD pattern of as-prepared silver particles. All the peaks from XRD pattern was accordance with

JCPDS Card No. 04-0783 and no impurities were observed, indicating the sample was silver crystal with high purity. Furthermore, the strong intensity of the peaks demonstrated good crystallinity of silver particles. Fig. 2. presented the SEM images of silver particles's surface morphology. It could be seen from Fig. 2, the silver particles dispersed uniformly with average size around 1.5 μm. According to report, the silver crystallites with diameter of 1-2 μm is appropriate for metallization contact. [19-21]
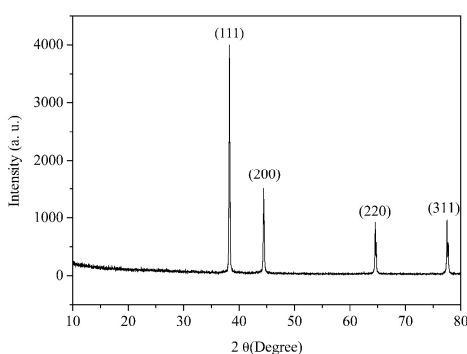
Figure 1 XRD pattern of silver particles obtained at optimal reaction conditions
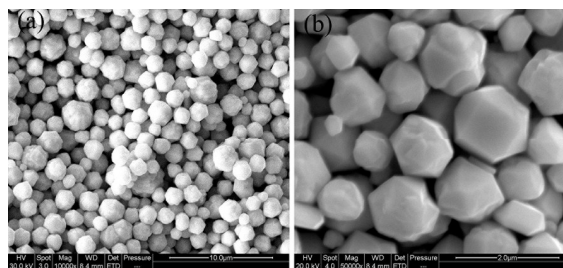


Figure 2 SEM image of silver particles prepared at optimal reaction conditions (a) Low resolution and (b) high resolution



**Effect of crystal structure of glass frits on Ag crystallites grown on Si substrate**

**Analysis of glass structure and effect on silver crystalline in glass layer**

Table 1 shows the different constituents of the glass-frit powders, named as GS-1, GS-2 and GS-3. The glass-frit powders were prepared by adding specific reagent that provided nucleation sites to facilitate the formation of the crystal structure, as shown in

Table 1 Experimental constituents of glass frit powers as GS-1, GS-2, GS-3.

| Glass frits | Constituent(mol%) | | | | | |
|---|---|---|---|---|---|---|
| | PbO | TeO$_2$ | SiO$_2$ | CaO | Al$_2$O$_3$ | Others |
| GS1 | 43 | 37 | 12 | 2 | 4 | 2 |
| GS2 | 43 | 37 | 9 | 2 | 2 | 7 |
| GS3 | 43 | 37 | 6 | 2 | 1 | 11 |

Fig. 3. The phase of the glass-frit samples was identified by XRD. As shown in Fig. 3, only a broad peak was detected at around 30° in the pattern of GS-1, indicating the material's amorphous structure. With the nucleation content increasing from 7% mol to 11% mol, GS-2 and GS-3 patterns had a little background due to the presence

of a part of glassy phase. Two different crystalline phases appeared in the glass structure that were confirmed to two kinds of TeO$_2$ (JCPDS No.41-0945 and JCPDS No.09-0433). The peak intensity of GS-3 was stronger than that of GS-2, which was ascribed to the excellent crystallization property resulted from the introduction of

more nucleation. According to the reactions proposed by Hong et al., [19] during the sintering process, the glass frit softened and melted first and then began to dissolve the silver particles. Upon further heating, the lead oxide of glass frit started to etch the silicon nitride layer via a redox reaction as below:

$$2PbO + SiN_x \rightarrow 2Pb + SiO_2 + N_2$$
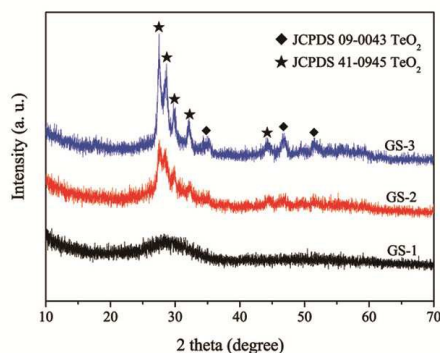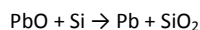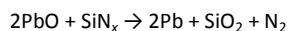
$$PbO + Si \rightarrow Pb + SiO_2$$



Figure 3  XRD patterns of amorphous glass GS-1 and crystalline glass GS-2 and GS-3

At the same time, the silver particles also sintered or coalesced according to interdiffusion of atoms between contacted metal particles. Finally, during cooling process, silver and lead separated according to the phase diagram and silver crystallized in the glass layer and silicon surface. As for the typical amorphous structure glass frit, the melting and cooling process was slowly and provided sufficient time for silver particles sintering and coalescing, which resulted in large silver crystallites during cooling process and increased probability of junction shunting for shallow emitters. During the firing step, silicon nitride layer was etched by PbO in glass frit and some silver crystallites embedded on silicon substrate to form metallization contact. Generally speaking, the depth of p-n junction is 100 nm,[15] when large crystalline silver penetrated the silicon substrate deeper than 100 nm, the p-n junction was broken down and resulted in the degradation of electrical properties. On the contrast, the crystalline glass accelerated the melting process and promoted its flowing, which tended to decrease the silver particles coalesce but allowed them to distribute uniformly in the glass layer.

Furthermore, the rapid crystallization of the crystalline glass frit could also freeze silver particles and prevent them form aggregating. As a result, smaller silver crystallites diffused into the glass layer and silicon emitter uniformly, which reduced the probability of junction shunting for shallow emitters. In addition, more silver precipitates in the glass could be in favor of metal-assisted tunneling through the glass layer. Therefore, the crystalline glass frit should have optimal ingredients for good metallization contacts.

**Investigation of crystalline glass frits' effect on silver-silicon contact**

In order to investigate the influence of glass structure on the silver crystallites distribution in the glass layer and the silicon substrate, the different kinds of glass frits (GS-1, GS-2, and GS-3) were mixed with the same silver particles and organic medium to prepare front-side silver pastes, denoted as GS-1a, GS-2b, and GS-3c for printing onto the silicon substrate to form the positive emitter. Fig. 4a, 4b, and 4c show the cross-sectional microstructures of solar cells fabricated with these silver pastes. In Fig. $4a_1$, $4b_1$, and $4c_1$, the bulk silver and glass layer were removed by chemical etching technique using aqua regia to expose the silver crystallites on the surface of the silicon substrate. As shown in Fig. $4a_2$, $4b_2$, and $4c_2$ after removing the silver crystallites by second chemical etching with 3% HF, some pits appeared on the silicon substrate as a result of Ag-crystallite penetration.

**ARTICLE**

Based on above understanding, a comparison of the cross-sectional microstructures of solar cells by SEM was displayed in Fig. 4. It could be seen clearly from Fig. 4(a) and (a₁), much large silver crystallites were distributed in the glass layer and embedded the silicon substrate, which would break-down the p-n junction and lead to electric leakage of solar cell. [10,15] The result proved by the big pits in the silicon substrate of Fig. 4(a₂). As for the GS-2, a large number of small silver crystallites distributed uniformly in the glass layer, as shown in Fig. 4(b) and 4(b₁). which offered conducting channels and mild etching to silicon substrate (Fig. 4(b₂) ), and met the requirement for good ohmic contact.[15] The result was confirmed by the shallower pits on the silicon emitter surface in Fig. 4(a₂) than Fig. 4(a₁). However, the sharp diffraction peaks indicated that the crystallinity of GS-3 increased substantially and further shorten the melting and cooling time. Therefore, much smaller crystalline silver particles were obtained compared with GS-2 (Fig. 4(c) and (c₁)). These smaller crystalline silver only precipitated but not penetrated the glass layer (Fig. 4 (c₂)), and then the effective metallization contact could not be acquired. A simple schematic illustration for the formation of metallization contact was presented in Fig. 5. Put simply, the GS-2 was the optimal crystal glass with appropriate proportion, which not only provided conducting channels but also mild etching to silicon substrate to form good ohmic contact.
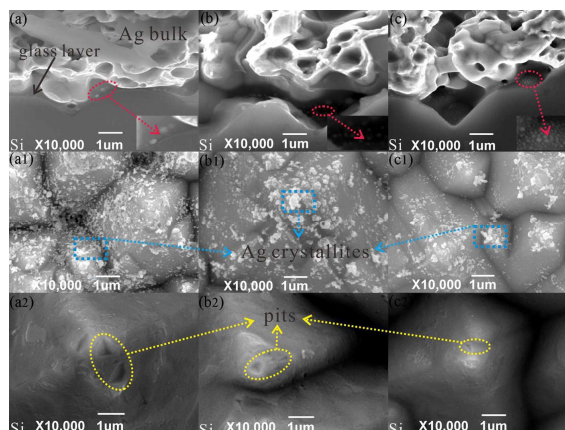


Figure 4 SEM images of being fired solar cells: (a, b, c) SEM cross section images of silver electrode, the insets displayed the silver crystallites distribution on the silicon substrates and glass layers; (a₁, b₁, c₁) SEM top-view images of c-Si solar cell after first chemically etched by aqua regia, demonstrated the silver crystallites attached to the surface of silicon substrate; and (a₂, b₂, c₂) SEM top-view images after second chemically etched by 3% HF to expose the surface of the emitter, some pits appeared on silicon substrate
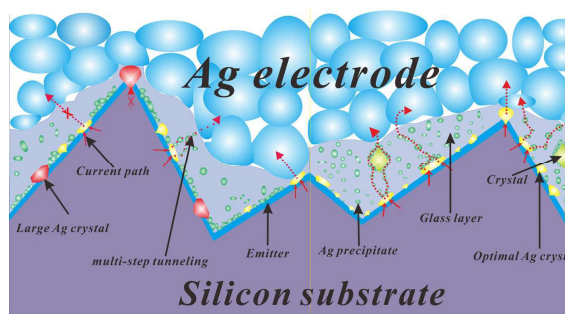


Figure 5 The mechanism schematic diagram of crystalline glass frit influences on the formation of electrode emitter

**Effect of particle size of glass frits on electrical properties of solar cells**

**Journal Name ARTICLE**

GS-2 was chosen to study the effect of particle size on solar-cell electrical properties. The cooled melt was ground by a planetary ball mill for different time to obtain glass-frit powders with different particle sizes. The size distribution of ground glass frit powders was plotted as a function of ball milling time (h). It was noticed that the size decreased gradually and then increased after 12 h ball milling due to the agglomeration. Based on the curve (Fig. 6) of ground glass-frit powders, we chose the powders that were ground for 6 h ($D_{90}$ = 7.57 μm), 8 h ($D_{90}$ = 4.94 μm), 10 h ($D_{90}$ = 3.12 μm), and 12 h ($D_{90}$ = 1.58 μm), hereafter referred to as GF-1, GF-2, GF-3, and GF-4, respectively. Front-side silver pastes were prepared using above glass frits and then screen printed on silicon wafers.
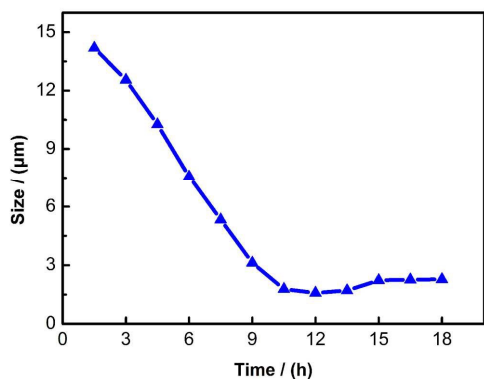


Figure 6 The change curve of glass frit's particle size decreased with the increasing of grinding time

In the high-energy ball-milling process, collision and squeezing between the glass frit and the zirconia grinding media changed the morphology of the glass-frit powder. The morphologies of glass frits after different ball milling time were shown in Fig.7 and the insets in top right corner were the size distribution of glass frits measured by laser particle analyzer. Fig. 7(a) displayed the morphology and particle size of GS-1 that experienced 6 h ball milling. It could be

seen clearly, large clumps of the glass-frit powder appeared and the average diameter of glass frit was 7.57 μm (D90) from the inset. It could also be seen from the inset, there was big difference between D10 (0.36 μm)and D90 (7.57 μm), indicating the glass frit particles distributed nonuniformly. After being ground for 8 h, the particle size of glass frit decreased dramatically to 4.94 μm (D90) and some fine particles appeared, while the big clumps and fine particles mixed together and resulted in the nonuniformly distribution, as shown in Fig. 7(b). As for the GF-3 after being ground 10 h, the large clumps disappeared completely in Fig. 7(c) and the particle size distributed uniformly with average diameter of 3.12 μm (D90). When the glass frit was ground for 12 h, as shown in Fig. 7(d), the particle size of glass frit decreased monotonously and became ultrafine powder with the average diameter 1.58 μm (D90). As the specific surface area increased, the particles intended to aggregate seriously during the firing step.
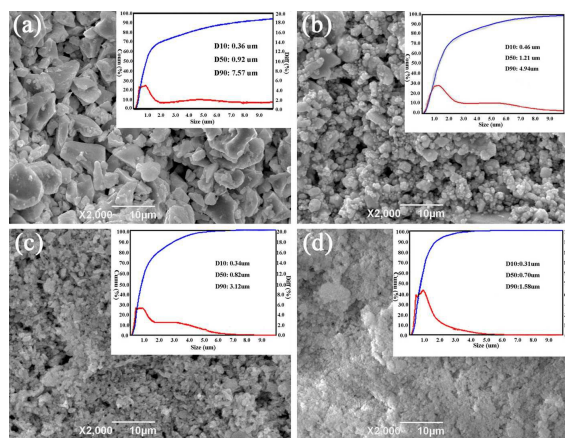


Figure 7 SEM images and particle size distribution of different glass frits: (a) GS-1; (b) GS-2; (c) GS-3; and (d) GS-4. The insets displayed the distribution of glass frit's particles size after different ball milling time

Fig. 8 showed plane-view images of silver fingers on the fired solar cells. Some holes could be observed clearly in Figs. 8a, b, and

d, exposing the bare silicon surface. Figs. 8a and b indicated that particles size of the glass frit was too large and could not match with the silver particles (1-2 μm), therefore, compact contact between glass frit and silver particles could not acquired and resulted in big holes in silver electrode. Because the particle size of GS-2 was smaller than GS-1, the smaller holes presented in GS-2. However, when the size of glass frit particles became smaller in GS-4, the particles tended to agglomerated seriously and decreased the specific surface area during the sintering process. The agglomeration of small glass frit particles also resulted in big holes in silver electrode, as demonstrated in Fig. 7 (d). As for the GS-3, the particles of glass frit was moderate and matched well with silver particles, meanwhile, the particles could not cause agglomeration during firing step. Therefore, the GS-3 with average diameter 3.12 μm (D90) was suitable for prepared silver paste and formatted the smooth and regular silver electrode without holes. In order to further testified the excellent of GS-3, a comparison of performance parameters of solar cells as shown in Fig. 9, including the conversion efficiency ($E_{ff}$), fill factor (FF), open-circuit voltage ($V_{oc}$), and series resistance ($R_s$), showed that silver electrode prepared with GS-3 led to high electrical resistivity and low conversion efficiency. Therefore, the optimal size of crystalline glass was 3.12 μm and distributed uniformly.
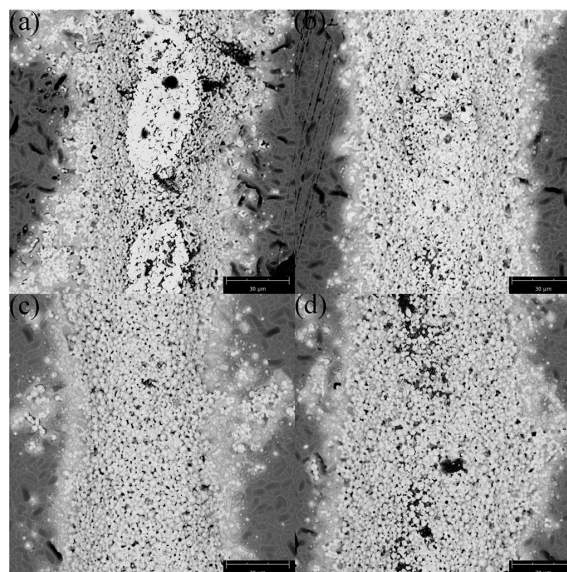


Figure 8  SEM images of front-side silver fingers screen printed by pastes contain glass frits: (a) GF-1; (b) GF-2; (c) GF-3; and (d) GF-4
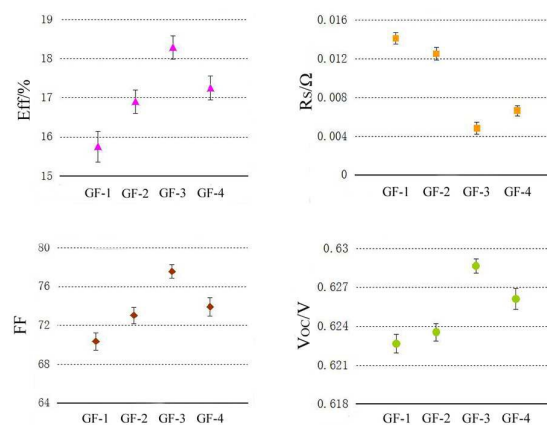


Figure 9  A comparison of performance parameters of solar cells: (a) conversion efficiency (Eff); (b) fill factor (FF); (c) open-circuit voltage (Voc); and (d) series resistance (Rs)

**Effect of glass-frit-powder content in paste on electrical properties of solar cells**

The as-prepared crystalline glass frit (GS-3) was mixed with a certain amount organic medium and silver particles to prepare a

**Journal Name ARTICLE**

series of front-side silver pastes with different contents of glass frit, as shown in Table 2. The glass frit decreased from 4.0 wt% to 2.0 wt%, which was donated as GJ1 to GJ5. The adhesion of the silver electrode prepared by different silver paste containing different content of glass frit (GS-3) were tested with FDV-50 force apparatus. The results was demonstrated in Fig. 10，the left bar graphs were the tensile force between silver electrodes and silicon substrates and the right were the silver electrodes experienced drawing by tension test. As Fig. 10 presented, when the glass-frit content in the paste was 2 wt% (GJ5), the adhesion was too low (1.26 N/mm$^2$) and the solder ribbon fell off easily without broken. As the content of GS-3 increasing to 3 wt% in GJ3, the viscosity of silver paste was moderate and bound the silver particles effectively to the silicon substrate, providing proper adhesion (3.39 N/mm$^2$) to ensure that the solder ribbon was firmly affixed to the wafer throughout the long working life of an encapsulated solar-cell panel. When the proportion of glass frit increased 4 wt% in GJ1, the tension break force reached 7.76 N/mm$^2$, which was too strong to result in the solar cell's fragment. Therefore, with the GS-3 content increasing in the silver paste, the tension between silver electrode

and silicon substrate increased subsequently. Although high adhesion was beneficial to prolong the working life of solar cells, the series resistance was also increased, lowering the conversion efficiency of the cells, as shown in Fig. 11. Hence, the 3.0 wt.% content of GS-3 in silver paste could not only provide moderate tension but also led to low series resistance, which was the optimal recipe.
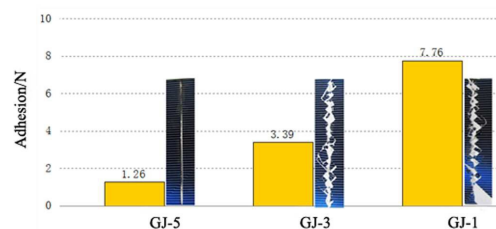


Figure 10 The change of Ag fingers' adhesion with increasing of glass frits contents. The left bar graphs were the tensile force between silver electrodes and silicon substrates, the right were the silver electrodes experienced drawing by tension test

Table 2 The different contents of composition in the paste to corresponding conversion efficiency

| Paste | Composition | | | |
| --- | --- | --- | --- | --- |
| | Silver particles (wt%) | Glass frits (wt%) | Organic medium (wt%) | Conversion efficiency ($E_{ff}$%) |
| GJ1 | 90 | 4.0 | 6.0 | 12.51 |
| GJ2 | 90 | 3.5 | 6.5 | 16.81 |
| GJ3 | 90 | 3.0 | 7 | 18.48 |
| GJ4 | 90 | 2.5 | 7.2 | 17.92 |
| GJ5 | 90 | 2.0 | 7.4 | 17.60 |

# Journal Name

## ARTICLE

A few reasonable assumptions can be proposed to explain the effect of glass frit on the adhesion of cells. The glass frit in the silver paste is melted first during firing, promoting the silver particles to melt rapidly. Hence, a paste with low glass-frit content cannot provide enough contact points to completely melt the particles. The main reason of decreased adhesion was that the solder ribbon could not be tightly welded to the fingers because the silver particles of some areas melted unevenly. With the glass-frit content increasing, the adhesion of fingers also gradually enhanced, demonstrating that more contact points for melting among silver particles offerred them a chance to integrate more easily. However, a thicker glass layer deposited on the silicon substrate due to high content of glass frit in the paste, and the photo-generated carriers cannot be transferred through glass layer and create a conducting channel from silicon substrate to silver electrode. Consequently, the adhesion is high enough with higher glass-frit content, while the electrical properties of the cells degrade, as shown in Fig. 11.
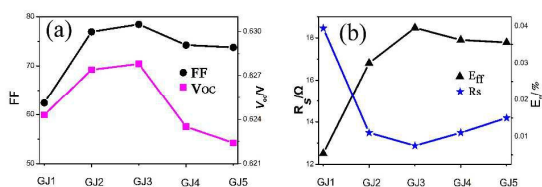


Figure 11   The electrical properties curves of solar cells screen printed by pastes GJ1, GJ2, GJ3, GJ4, and GJ5

It could be deduced that a low glass-frit content of 2.0-2.5 wt% in the silver paste provided an insufficient liquid phase to wet the silver particles. The dense fingers could not be formed because of the low driving force. Hence, the nonuniform silver crystallites appearing on the silicon substrate would not draw and collect electrons smoothly and resulted in high series resistance. When the glass-frit content increased to 3.5-4.0%, dense fingers were formed during sintering because the silver particles melted completely. Fig. 11 showed that these parameters were not ideal, however, it was well known that the amount of silver crystallites formed on the Si substrate was determined by the glass frit in the paste. A large amount of silver crystallites were beneficial in drawing and collecting electrons. However, a thicker glass layer precipitated between the silicon substrate and the bulk silver with glass frit content increasing, which blocked the electrons from being drawn owing to the absence assisted multi-step tunneling in the glass layer. Meanwhile, the thick glass layer reduced the probability of contact between the silver crystallites and the bulk silver. Our results showed that around 3 wt% of glass frit in the silver paste yielded to the excellent electrical properties of solar cells.

## Conclusions

As an important component in silver paste, Glass frit powder played a significant role in the formation of Ag-Si contacts in crystalline-silicon solar cells. Glass frits with different degrees of crystallization were prepared by introducing a nucleating agent to provide nucleation sites for formation of the crystal structure.

**RSC Advances**

Journal Name ARTICLE

Through SEM observations of the cross-sectional and surface microstructures of solar cells, it was speculated that a glass frit with moderate crystallization could control the growth and distribution of silver crystallites in the glass layer and silicon substrate, which was facilitated to form conduct tunneling and optimal etching condition to silicon substrate. Meanwhile, it could be seen from optimization of the parameters that 3 wt% of glass frit with a particle size of 3.12 μm in the silver paste ensured the best electrical performance of solar cells. Therefore, the preparation of crystalline glass frit with different diameters and proportions provided a new way for improving the conversion efficiency of solar cell.

## Acknowledgements

## Notes and references

1  Zhou, J., Gan, W., Li, Y., Huang, B. and Yang, C., *J. Mater. Sci.-Mater. El.*, 2015, **26,** 234-241.

2  Wang, J., Zhou, L., Zhu, H., Yang, R., Zhou, Y., Liu, L. and Chen, J., *Photon. Res.*, 2015, **3**, 58-62.

3  Zheng, G., Tai, Y., Wang, H. and Bai, J., *J. Mater. Sci.-Mate.r El.*, 2014, **25,** 3779-3786.

4  Wu, J., Cao, P., Pan, T., Yang, Y., Qiu, C., Tremblay, C. and Su, Y., *Photon. Res.*, 2015, **3,** 9-14.

5  Li, W., Wu, T., Jiao, R., Zhang, B. P., Li, S., Zhou, Y. and Li, L., *Colloid Surface A*, 2015, **466,** 132-137.

6  Beatrix Blank, Carolin Ulbrich, Tsvetelina Merdzhanova, Christoph Zahren and Bart E. Pieters, *Sol. Energy Mater. Sol. Cells,* 2015, **143,** 1-8.

7  Tsai, J. T. and Lin, S. T., *J. Alloy Compd.,* 2013, **548,** 105-109.

8  Huh, J. Y., Hong, K. K., Cho, S. B., Park, S. K., Lee, B. C. and Okamoto, K., *Mater. Chem. Phys.,* 2011, **131,** 113-119.

9  Ionkin, A. S., Fish, B. M., Li, Z. R., Lewittes, M., Soper, P. D., Pepin, J. G. and Carroll, A. F., *ACS Appl. Mater. Interfaces,* 2011, **3,** 606-611.

10  M.M. Hilali, S. Sridharan, C. Khadilkar, A. Shaikh, A. Rohatig and S. Kim, *J. Electron. Mater.,* 2006, **35,** 2041-2047.

11  Enrique Cabrera, Sara Olibet, Joachim Glatz-Reichenbach, Radovan Kopecek, Daniel Reinke and Gunnar Schubert, *J. Appl. Phys.,* 2011, **110,** 114511.

12  Lin, C. H., Tsai, S. Y., Hsu, S. P. and Hsieh, M. H., *Sol. Energy Mater. Sol. Cells,* 2008, **92,** 1011-1015.

13  E.Cabrera, S.Olibet, J.Glatz-Reichenbach, R.Kopecek, Daniel Reinke and Gunnar Schubert, *Energy Procedia*, 2011, **8,** 540-545.

14  Dong-Youn Shin, Jun-Young Seo, Hyowon Tak and Doyoung Byu, *Sol. Energy Mater. Sol. Cells,* 2015, **136,** 148-156.

15  C. Ballif, D. M. Huljić, G. Willeke and A. Hessler-Wyser, *Appl. Phys.Lett.,* 2003, **82,** 1878-1880.

16  Li, Z. G., L. Liang, and L. K. Cheng, *J. Appl. Phys.,* 2009, **105,** 066102.

17  Alex S. Ionkin, Brian M. Fish, Zhigang Rick Li and Liang Liang, *Sol. Energy Mater. Sol. Cells,* 2014, **124,** 39-47.

18  Z. G. Li, L. Liang, A. S. Ionkin, B. M. Fish, M. E. Lewittes, L. K. Cheng and K. R. Mikeska, *J. Appl. Phys.,* 2011, **110,** 074304.

19  Hong, K. K., Cho, S. B., You, J. S., Jeong, J. W., Bea, S. M. and Huh, J. Y., *Sol. Energy Mater. Sol. Cells,* 2009, **93,** 898-904.

20  Guiquan Guo, Weiping Gan and Feng Xiang, *J. Mater. Sci. Mater. Electron.,* 2011, **22,** 527-530.

21  Jung-Ting Tsai and Shun-Tian Lin, *J. Alloy. Compd.,* 2013, **548,** 105-109.